Computational Materials Science 95 (2014) 149–158

Contents lists available at ScienceDirect

Computational Materials Science

journal homepage: www.elsevier.com/locate/commatsci

Numerical simulations and modeling of the stability of noble gas atoms in interaction with vacancies in silicon

L. Pizzagalli [a,*], A. Charaf-Eddin [b], S. Brochard [a]

[a] Institut P', CNRS UPR 3346, Université de Poitiers, SP2MI, BP 30179, Boulevard Marie et Pierre Curie, 86962 Futuroscope Chasseneuil Cedex, France
[b] CEISAM CNRS UMR 6230, Université de Nantes, 2 rue de la Houssinière, BP 92208, 44322 Nantes Cedex 3, France

ARTICLE INFO

Article history:
Received 2 April 2014
Received in revised form 2 July 2014
Accepted 7 July 2014

Keywords:
Noble gas
Silicon
Density functional theory

ABSTRACT

In order to identify the main actors during the initial steps of the formation of noble gas filled bubbles, we have performed an extensive investigation of a single noble gas atom (helium, neon, argon, krypton, xenon) as interstitial or in interaction with a monovacancy and a divacancy in silicon. Density functional calculations in the generalized gradient approximation allowed us for determining the structure and stability of various configurations. We found that interstitial configurations are especially relevant for helium, and to a lesser extent for neon. Heavy noble gas species are predicted to form complexes with vacancies, except in out-of-equilibrium situations where an original bond-centered interstitial configuration is favored. Besides, we propose a model combining a repulsive interaction between the host local electronic density and the noble gas atom, and an elastic description of this atom as a deformable spherical inclusion into an homogeneous isotropic medium. This model is shown to provide an appropriate description, especially for light noble gas species such as helium and neon.

1. Introduction

Chemical elements located in the rightmost column of the periodic classification constitute the group of so-called noble gas (NG) species. They are, among other specific properties, characterized by the quasi absence of chemical reactivity, because of their completely filled electronic shells. Being inert, NG exhibit unique behaviors when interacting with many materials [1]. For instance, NG can be used for processing semiconductors, yielding inert atmosphere during growth, ion beam milling of surfaces, or plasma etching. In electronics, light NG such as He or Ne are also potentially useful in the gettering process for electronic devices [2]. NG atoms are initially implanted in the material, far from the active layers of the future device. Subsequent treatments lead to the formation of cavities [3], which are then used to trap undesirable impurities migrating from active layers. The formation of these extended defects is beneficial for relaxing strain in pseudomorphic SiGe/Si heterostructures, and is also an essential step in the smart-cut process used in the production of silicon-on-insulator wafer substrates. In a spatial context, embedded NG atoms have been found in interstellar dusts [4], and can be used as marker for models attempting to describe stars evolution. Finally, the effects of the presence of NG into materials are also extensively investigated in the context of nuclear applications. In fact, NG like helium are produced in large quantities coming from neutron-induced transmutation reactions and from the coolant. In fusion reactors, the plasma is also generating a high flux of helium which will interact with the wall. The accumulation of helium into structural, confining or fuel cladding materials leads to the formation of extended defects like bubbles [1,5], potentially resulting in swelling, embrittlement, surface roughening, blistering, all processes that can dramatically degrade the mechanical properties.

Extended defect formation due to the presence of helium is largely documented in metals [6,7], covalent systems like silicon [8–14], silicon carbide [15–19], gallium nitride [20], or disordered materials [21]. However a similar outcome has been observed when other NG species such as neon [22,23], argon [24–28], krypton [29,30], and xenon [26,31–33] are inserted into materials. The formation of extended defects such as bubbles or platelets is then clearly a general feature caused by the presence of NG atoms into materials.

The generally accepted driving force behind defects formation is the non-solubility of NG atoms in most materials because of their chemical inertness. NG atoms tend to aggregate to lower the energy cost, occupying available space at defects or generating some if possible. As a result, the formation of NG-filled extended defects such as platelets and bubbles is generally favored.

* Corresponding author.
E-mail address: Laurent.Pizzagalli@univ-poitiers.fr (L. Pizzagalli).

http://dx.doi.org/10.1016/j.commatsci.2014.07.011
0927-0256/

Nevertheless, the different and possibly complex mechanisms leading to the formation of these defects are not fully understood yet. For instance NG-filled bubbles can grow through continuous supplies of NG atoms and vacancies, by coalescence of existing bubbles, or by emission of dislocation loops [6,34]. Determining the properties and evolution of NG-filled bubbles was the motivation of a large number of dedicated studies. A key property in all proposed models is the NG density into the bubble, which can be obtained thanks to experiments [32,35–40] and numerical simulations [41–50].

To understand bubbles formation, it is also equally important to determine the very first steps leading to the formation of bubbles precursors. Then elementary properties such as formation and migration energies associated with single NG atoms need to be characterized. Furthermore, one has to consider the interaction of NG atoms with vacancies. In fact, NG atoms can be introduced into materials only as energetic particles. A large part of this energy is dissipated through inelastic collisions of the impinging particle with electrons, and the remaining part as elastic collision with ions of the host material. When the energy transmitted to one of these ions is higher than the threshold displacement energy [51–54], there is formation of both an interstitial and a vacancy defect (a Frenkel pair). A large proportion of those recombine during the irradiation process [55,56]. Nevertheless, it is assumed that a non negligible amount of vacancy defects remain, whose interaction with NG atoms could play the role of precursors for bubbles formation. This is especially true for the heaviest NG species, for which a larger amount of damage is created in the host lattice.

In diluted state, NG atoms are hardly detected by most of experimental techniques because of the lack of interaction with the host lattice. Then, available information concerning NG interstitials alone or in interaction with vacancies is often obtained from theoretical studies. Helium impurities have been the most studied, especially in metals [57–67], but also in more complex materials such as oxide [68] and MAX phases [69]. In covalent materials, single NG atom properties have been investigated especially for helium in several group IV materials such as silicon [70–74], silicon carbide [75–78], and diamond [79]. In these studies, it appears that it is usually favorable for helium to bind to existing vacancies. For heavier NG species, such as Ne, Ar, Kr and Xe, both experimental and theoretical data are scarce. Further investigations are then needed to extend the current state of the art.

In this paper, we report density functional theory (DFT) calculations of the properties of single NG atoms (He, Ne, Ar, Kr, and Xe) as interstitial or in interaction with mono- and divacancy in silicon. The latter was chosen since it is considered as a covalent model material, for which one can hope that the results presented here will be quite general. In a first part, we describe our calculations of the stability and structure of a NG atom as interstitial and in presence of vacancies. In a second part, we propose a simple model combining an elastic description and an electronic embedding contribution, which allows for reproducing the results of numerical simulations.

2. Methods

The calculations reported in this work were performed with the PWscf code [80] from the Quantum-ESPRESSO project [81], therefore in the framework of DFT [82,83], and using the Perdew–Burke–Ernzerhof (PBE) [84] generalized gradient approximation for the description of exchange and correlation. The use of a DFT-PBE framework is justified here because the interactions between the NG atoms and the host materials are essentially repulsive. Furthermore, PBE has been shown to allow an overall better modeling of weak bonding than other usual exchange–correlation approximations [85]. The interaction between valence electrons and ions was described using ultrasoft pseudopotentials [86]. Wave functions were expanded on a plane-wave basis, with an energy cutoff of 15 Ry. Within these conditions, the computed lattice parameter of silicon a_0 was found to be equal to 5.468 Å, in good agreement with the experimental value of 5.43 Å. The calculation of the electronic density was made by sampling the Brillouin zone with a $\frac{1}{2}$-shifted 2^3 Monkhorst–Pack grid of k-points [87], equivalent to a set of 4 irreducible k-points.

A $3a_0 \times 3a_0 \times 3a_0$ periodically repeated cubic supercell, including 216 atoms for a perfect silicon crystal, was used for all simulations. A NG atom was initially positioned at different locations in the perfect lattice, or relative to a mono- or a divacancy. Forces were relaxed using the Broyden-Fletcher-Goldfarb-Shanno quasi-Newton algorithm, stopped when residual forces were below 10^{-3} eV Å^{-1} to ensure well converged final structures.

Several sources of errors are possible when dealing with finite size density functional calculations. An important one is related to the convergence of the electronic structure calculation. Here we found that both the chosen energy cutoff and k-points set were appropriate to obtain well converged energies, with errors likely to be much lower than the influence of the exchange correlation approximation selected in our work. Another important source of error is coming from the use of a finite size cell, especially for the heaviest NG species which can induce important lattice deformations. The influence of using fixed volume calculations can be estimated by computing an Eshelby type elastic correction, following Hepburn et al. [66]. For Xe in tetrahedral interstitial position, for which the lattice distortions are the largest among investigated configurations, we calculate a correction of 0.3 eV, thus only 3% of the 10.22 eV formation energy (see Table 1). Corrections will be much lower for lighter NG species or configurations involving NG in vacancies. Finally, zero point energy contributions have not been computed in this work, since they have been shown to change excess energies by about 0.01 eV [66]. Overall, we estimate the errors on our computed excess energies to be at least 0.05 eV and at most 3%.

The validity of our computational setup was finally assessed in the case of the mono and divacancy in silicon. The formation energies in both cases are

$$E_f(V_1) = E(V_1) - \frac{N-1}{N}E_0 \quad (1)$$

$$E_f(V_2) = E(V_2) - \frac{N-2}{N}E_0 \quad (2)$$

where $E(V_1/V_2)$ is the total energy of the defected configuration, N the total number of atoms and E_0 the total energy of the pristine system. These definitions allow for an appropriate cancelation of errors associated with the finite size of supercells. We calculated a formation energy of 3.33 eV for the monovacancy, in excellent agreement with previous investigations [88–90]. The relaxed

Table 1
Energies (in eV) required to introduce a single NG atom into the silicon lattice according to different configurations (see the text for labels meaning). The '–' symbol indicates unstable or untested configurations.

	He	Ne	Ar	Kr	Xe
T	1.00	2.50	5.83	7.14	10.22
H	1.66	3.37	6.86	8.02	10.82
BC	–	–	5.81	5.82	7.14
SP	–	–	7.13	6.96	–
V_1S	1.82	1.98	2.63	2.29	3.34
V_1T	1.15	1.65	–	–	–
V_2S	–	–	1.63	1.24	2.30
V_2C	0.49	0.89	–	1.94	2.54

structure exhibits the correct D_{2d} symmetry [89,90], with bond lengths of 2.97 Å and 3.52 Å in the core of the defect. A formation energy of 5.05 eV is obtained for the divacancy, which gives a binding energy of 1.61 eV for two monovacancies, also in excellent agreement with previous works [91–93].

3. Structure and stability

Silicon crystallizes in the cubic diamond lattice, an open structure with several possible interstitial sites (Fig. 1). High symmetry locations are the so-called tetrahedral (T) and hexagonal (H) sites. When positioned in the former, an interstitial has 4 silicon neighbors at a distance of $\sqrt{3}a_0/4 \simeq 0.433a_0$, which is the 1st neighbors distance of the cubic diamond lattice. In the second case, an interstitial would have 6 silicon neighbors at a distance of $\sqrt{11}a_0/8 \simeq 0.414a_0$. Another possible location is the bond-centered (BC) site, the interstitial atom being positioned between two first-neighbor silicon atoms. This configuration, untested for NG as far as we know, is favored for atomic hydrogen [94,95]. Finally, Goss and co-workers reported that in diamond a single argon, krypton or xenon atom would preferably form ⟨001⟩-oriented split interstitials [79]. This configuration, tested here for the same NG species, is called SP in the following. In the presence of a monovacancy, an obvious location is the center of the vacancy, where a NG impurity can be thought to be substitutional (V_1S). Other possible positions are T and H sites in the immediate vicinity of the vacancy. Finally, high symmetry sites in presence of a divacancy are the mid-position between the two vacancies (V_2C), or the center of one of the two vacancies forming the divacancy (V_2S).

To determine the most stable locations for a NG atom, we computed the insertion energy needed to introduce a NG atom into the silicon lattice, in presence or not of vacancies, as

$$E_i(NG,X) = E(NG,X) - E(X) - \mu(NG) \quad (3)$$

with $E(NG,X)$ the total energy of silicon in state X (pristine, with V_1 or V_2) and containing a NG atom, $E(X)$ the total energy of the system in state X without the NG atom, and the reference energy μ of the NG atom. In this work, μ is chosen equal to the total energy of the NG atom alone computed in the same supercell.

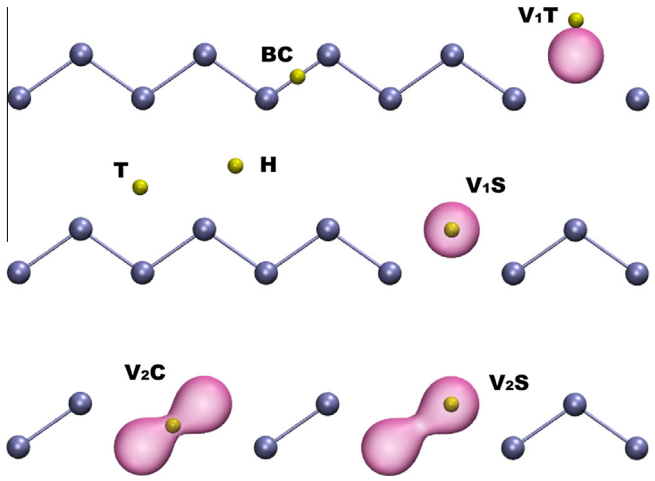

Fig. 1. Some possible configurations for a NG impurity (yellow sphere) as interstitial or in interaction with mono- and divacancies (transparent pink volume), projected in a {110} silicon (blue spheres) layer. See Section 3 for further explanations on notations. (For interpretation of the references to colour in this figure legend, the reader is referred to the web version of this article.)

3.1. Helium

Investigating first interstitial configurations, the tetrahedral T site is the most stable site for helium with $E_i = 1.00$ eV (Table 1 and Fig. 2), a value in the range of published data [70,72–74]. The final structure keeps the original T_d symmetry, with distances between helium and first-neighbors silicon atoms enlarged by only 3.3% during the relaxation. Slightly lower deformations were previously reported, probably because of smaller computational systems [70,72–74]. Helium is found to be unstable in the hexagonal H site, migrating towards the T site during the structural relaxation. Constraining the helium atom to remain in H, an insertion energy of 1.66 eV is obtained, in agreement with two previous works [70,74]. It has been suggested that the significantly higher value reported in Ref. [72] might be due to the use of a different theoretical framework, and also of a very small computational system [74]. The latter is probably the right explanation, since discrepancies tend to increase for heavier NG impurity, as will be seen in the following. In our case, the deformation of the silicon lattice in the vicinity of the helium atom remains small, distances between helium and first-neighbors silicon atoms being stretched by 4.4%. Finally, we found that when the helium atom is initially positioned in the BC site, it migrates to the nearest T site during the relaxation.

A high insertion energy of 1.82 eV is obtained when the helium atom is located in the monovacancy center, in V_1S configuration (Table 1). This energy is higher than the value of 1.4 eV reported by Zavodinsky et al. [73]. Other investigations reported that this configuration is not stable [70,72]. This disagreement could be simply explained by considering the initial structure used for simulations. If the helium atom is positioned in an unrelaxed vacancy, it is trapped during relaxation because of the T_d symmetry. Instead, if the initial configuration is a helium atom located in a relaxed vacancy, thus characterized by a D_{2d} symmetry, the V_1S configuration becomes unstable. In the latter case, the helium atom migrates towards the T site first neighbor of the vacancy (Table 1 and configuration T1 in Fig. 3). The final separation between the helium atom and the vacancy is 1.75 Å, and the maximum lattice distortion is supported by the silicon atom on the other side of the vacancy, which is shifted by 0.78 Å. The final energy is 1.15 eV, thus 0.15 eV higher than for interstitial helium. This energy difference is exactly the same as reported in the seminal work by Alatalo et al. [70]. We found another stable helium configuration T2 in the vicinity of the vacancy, with an insertion energy of 1.25 eV. This structure, shown in the Fig. 3, is obtained when the helium atom is initially located in a T site second neighbor to the vacancy. The relaxation brings the helium atom at a distance of 1.32 Å of the monovacancy center. However, when initially positioned in a T site third neighbor to the vacancy, the helium atom remains on site,

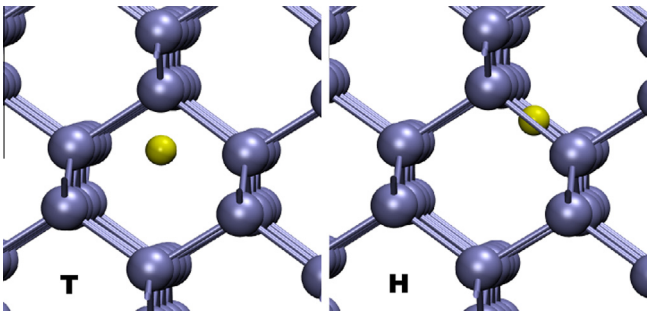

Fig. 2. Relaxed ball-stick structures for an interstitial helium atom in T and H sites, obtained from DFT-PBE calculations. Si (He) atoms are represented by blue (yellow) spheres with arbitrary radii. (For interpretation of the references to colour in this figure legend, the reader is referred to the web version of this article.)

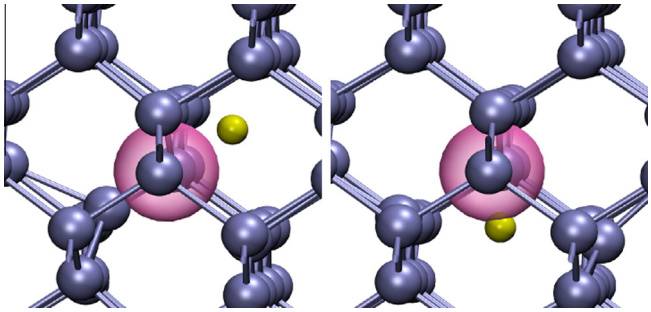

Fig. 3. Relaxed ball-stick structures (T1, left, and T2, right) for an interstitial helium atom in the vicinity of a vacancy, obtained from DFT-PBE calculations. Si (He) atoms are represented by blue (yellow) spheres with arbitrary radii. The monovacancy region is shown as a transparent pink volume. (For interpretation of the references to colour in this figure legend, the reader is referred to the web version of this article.)

with a negligible vacancy-helium interaction. Finally, it is found that for all monovacancy-related configurations the insertion energies are equal or higher than for the interstitial helium in pristine bulk, which confirms that a vacancy is a repulsive center [70,72,73]. Possible non-exclusive explanations are (1) the relaxation of the monovacancy towards the D_{2d} most stable state is blocked by the presence of the helium atom (2) the high electronic density in the vacancy center, due to the four dangling bonds, is not energetically favorable for a closed-shell atom like helium. This issue will be further investigated in the Section 4.

A low energy of 0.49 eV is needed to insert the helium atom in the center of a divacancy (Table 1), a significantly lower value than previously reported [72]. The relaxed structure exhibits negligible differences with the bare divacancy configuration, which would indicate that this energy is essentially due to the repulsive interaction between the helium atom and the electrons in the center of the divacancy. The second tested case with helium initially located at the center of one of the two vacancies (V_2S) is not stable, the helium atom relaxing towards the center of the divacancy. The lower insertion energy compared to the interstitial configuration clearly indicates that the silicon divacancy, unlike the monovacancy, is a trap for the helium atom. Furthermore, the presence of the helium atom increases the stability of the divacancy against dissociation. This configuration could then be considered as a precursor for helium-filled bubbles in silicon, as previously proposed by Raineri et al. [96]. However, recent molecular dynamics simulations suggested that large vacancy clusters are formed before helium is trapped [49], which would minimize the role of the helium-divacancy complex.

3.2. Neon

There have been fewer investigations of neon in silicon, compared to helium. Earlier calculations by Estreicher et al. revealed insertion energies larger than 3 eV for the interstitial configuration [72]. It is also predicted in this work that the monovacancy does not trap the neon atom, unlike the divacancy. This is not confirmed by recent theoretical investigations, which yield much lower insertion energies [74,97], and also show that the helium will be trapped by the monovacancy.

We first investigated the most stable configuration for an interstitial neon atom in pristine silicon, among the same three possible sites than for helium. The calculated insertion energies, reported in the Table 1, are typically 1.5 eV larger compared to the helium ones and keep the same ordering. The most stable configuration corresponds to the T site, with $E_i = 2.50$ eV. This value is 1.1 eV lower than the one published in the Ref. [72]. The final structure keeps the original T_d symmetry, the separations between the neon atom and the silicon neighbors being enlarged by 5%. Like for helium, a neon atom initially located in the H interstitial site migrates towards a T position during relaxation. A constrained calculation yields $E_i = 3.37$ eV, with a 7.6% increase of the distance between the neon atom and first-neighbors silicon. The last investigated interstitial site, BC, does not lead to a stable relaxed structure, like in the helium case.

Considering now defected silicon, we determined an insertion energy of 1.98 eV (Table 1) when the neon impurity is located at the center of a monovacancy. This configuration is only weakly stable, and the neon atom leaves this site when slightly displaced. Further relaxations make the system to evolve towards a configuration similar to the T2 structure represented in the Fig. 3. Note that when the neon atom is initially positioned in a T site first neighbor to the monovacancy (configuration T1 in the Fig. 3), it also relaxes to T2. The final neon-monovacancy distance is 1.18 Å, and the corresponding energy is only 1.65 eV. This energy is lower than the interstitial energy by 0.85 eV, which suggests that the neon atom will be trapped by the monovacancy. A similar conclusion can be drawn for the divacancy case. In fact, the most stable configuration is obtained when the neon atom is located in the center of the divacancy, with an insertion energy of 0.89 eV (Table 1). Like for helium, a silicon divacancy is therefore a trap for the neon atom. At last, the configuration with the neon atom positioned in V_2S is not stable.

3.3. Argon

The available knowledge regarding elementary properties such as energetics and configurations of a single argon atom in silicon is as scarce as for neon. The only available theoretical investigation concluded that a single argon in pristine silicon would be located in T site, with a large insertion energy of about 11.3 eV [72]. It is also predicted from this work that the argon atom would prefer to stay outside of a monovacancy, while the center of the divacancy is its most stable location.

Our calculations first revealed a picture qualitatively similar to what was obtained for helium and neon interstitials, that is a stable configuration in T site, and a weakly stable configuration in the H site. The corresponding insertion energies of 5.83 eV and 6.86 eV (Table 1) are about half the previously reported values [72]. The relaxed T structure is characterized by a maximum stretching of 8.8% for bonds between the argon interstitial and silicon atoms first neighbors. For the H configuration, the distance between the argon atom and the nearest silicon atoms increases by 12.7% during relaxation. However, the configuration with Ar in the BC site becomes now an interesting alternative to the usual T site. In fact, it is now a stable configuration, with an insertion energy of 5.81 eV. The relaxed structure is shown in the left part of the Fig. 4. The presence of the Ar atom leads to the breaking of the Si-Si bond, the two silicon atoms being shifted away by 1.39 Å from their initial positions while remaining aligned together with the Ar atom. Note that the small energy difference between T and BC configurations is within the uncertainty range of our calculations. Taking into account finite temperature effects could maybe widen this difference, but in the current state we can only conclude that both configurations could co-exist. Finally, we also tried to position the argon atom so as to form a ⟨001⟩-oriented split interstitial with a silicon atom (SP). This configuration is found to be stable, but is quite unlikely due to a high insertion energy of 7.13 eV (Table 1). The relaxed structure is characterized by a separation of 3.17 Å between the argon and the silicon atoms, and also by two other silicon atoms which are largely displaced. These atoms are all contained in a {110} plane.

In presence of a monovacancy, the most stable configuration is obtained with the argon atom now at the center, i.e. V_1S (right

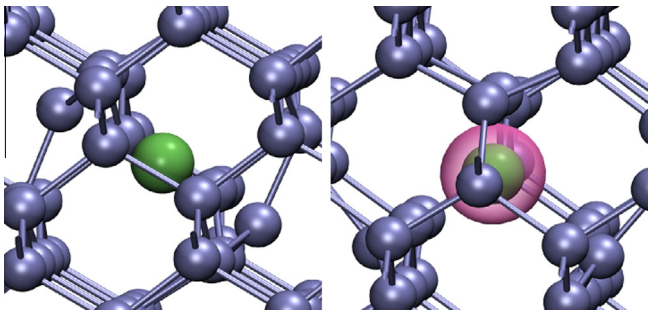

Fig. 4. Relaxed ball-stick structures for an argon atom in an interstitial BC site (left), and at the center of a monovacancy (V_1S, right), obtained from DFT-PBE calculations. Si (Ar) atoms are represented by blue (green) spheres with arbitrary radii. The monovacancy region is shown as a transparent pink volume. (For interpretation of the references to colour in this figure legend, the reader is referred to the web version of this article.)

panel, Fig. 4). Compared to the cases of helium and neon, other sites close to the monovacancy are not stable, the argon atoms relaxing to the center. The calculated insertion energy is 2.63 eV, thus much lower than both T and BC interstitial energies. The final relaxed structure is characterized by a large 0.69 Å displacement of the four first-neighbors silicon atoms away from the vacancy center, thus keeping the original T_d symmetry. These silicon atoms appear to be in a sp^2 hybridized state, forming three coplanar bonds with other Si atoms and with 120° bond angles.

Considering now the divacancy, we found only one stable configuration corresponding to the argon atom at one of the vacancy centers, with an insertion energy of 1.63 eV. This configuration is also obtained after relaxation when the argon atom is initially positioned in the center of the divacancy. The final structure is represented for the case of krypton in the left panel of Fig. 5. The three silicon atoms first-neighbors of the occupied vacancy center are shifted away from the argon atom during the relaxation, leading to a final geometry comparable to what is obtained in the monovacancy case (except the missing fourth atom removed to create the second vacancy). Also the dangling bonds of the unoccupied vacancy are partially reconstructed, with the creation of weak bonds between silicon atoms first-neighbors of the vacancy center.

Comparing the different calculated insertion energies clearly reveals that both mono- and divacancies are strong attraction centers for an argon atom (Fig. 6). Argon implantation usually generates a non negligible amount of damage in the silicon lattice, leading to a supersaturation of vacancies. Most of the implanted argon atoms are then likely to be trapped by these vacancies, be it in the implanted state or during annealing stages. Since the insertion energy for interstitial argon is large, it also becomes interesting to investigate whether a process involving the thermal formation of a mono- or divacancy at the impurity location might be energetically favorable. In the Fig. 6, we compare the interstitial insertion energy to the sum of the substitutional insertion energy plus the mono- or divacancy formation energy. Very close values are obtained in the case of the monovacancy formation, implying that a population of substitutional argon atoms would co-exist with a population of interstitial argon atoms at thermal equilibrium in pristine silicon. It also hints that bubbles formation might be initiated without the need for vacancies created during implantation.

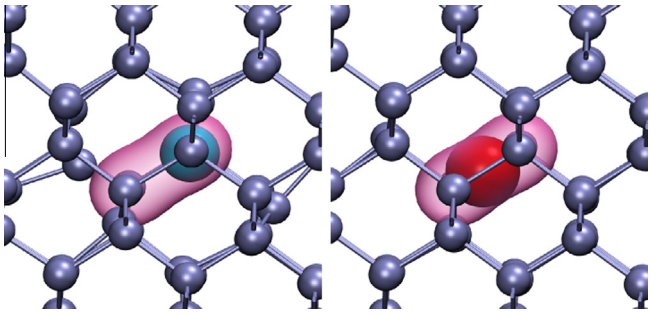

Fig. 5. Relaxed ball-stick structures for a krypton atom in V_2S configuration (left), and a xenon atom in V_2C configuration (right), obtained from DFT-PBE calculations. Si, Kr, and Xe atoms are represented by blue, cyan, and red spheres respectively, with arbitrary radii. The divacancy region is shown as a transparent pink volume. (For interpretation of the references to colour in this figure legend, the reader is referred to the web version of this article.)

3.4. Krypton

For krypton, it was also predicted that the NG atom is stable in the divacancy center but not in the monovacancy center, and that the most stable interstitial configuration corresponds to the krypton atom in the T site, with an insertion energy of 16.2 eV [72].

Instead, for the interstitial case, we found that the lowest insertion energy value of 5.82 eV is obtained for the krypton atom in the BC site (Table 1). In the relaxed structure (shown in the Fig. 4 for argon), the two silicon atoms near the krypton atom have been shifted away by 1.45 Å from their initial positions. Higher insertion energies of 6.96 eV, 7.14 eV and 8.02 eV have been computed for the SP, T and H configurations, respectively, suggesting that their occurence will be limited.

The krypton atom, like the argon atom, prefers to remain in the center of a monovacancy, in disagreement with the early calculation [72]. Our calculated insertion energy is only 2.29 eV (Table 1). Considering now the divacancy, the most stable configuration is obtained when the krypton atom is located in one of the vacancy centers (V_2S) with $E_i = 1.24$ eV. The relaxed system geometry is shown in the Fig. 5. Finally, a stable structure is also obtained when it is initially positioned at the divacancy center ($E_i = 1.94$ eV), unlike argon.

Then, it is straightforward to conclude that both mono- and divacancy are traps for a single krypton atom. If we now make the same energy analysis than for argon, it is found that the thermal formation of a monovacancy in the vicinity of a krypton interstitial could be energetically favorable (Fig. 6). The probability of

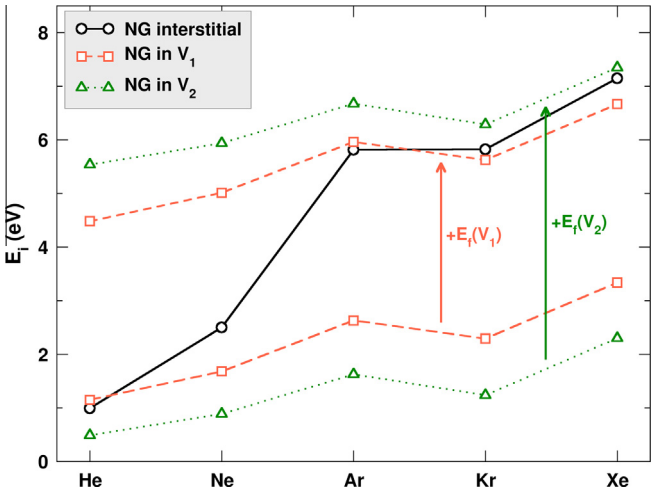

Fig. 6. Energies required to introduce a NG atom in bulk (black circles), mono (lower red squares) and divacancy (lower green triangles) in silicon. Only the most stable configurations are considered in each case. The upper red squares and green triangles are obtained by adding the formation energy associated with the mono and divacancy, respectively. (For interpretation of the references to colour in this figure legend, the reader is referred to the web version of this article.)

krypton atoms in interstitial state in silicon then appears to be smaller than for argon.

3.5. Xenon

The last investigated NG species is xenon, which is the heaviest and a priori the hardest to accommodate in the silicon lattice. Therefore, one can expect results in line with argon or krypton cases. In fact, the most stable interstitial configuration is obtained with the xenon in BC site ($E_i = 7.14$ eV, Table 1). The two nearest silicon atoms are now pushed away by 1.55 Å from their initial positions, the distance between the xenon atom and one of the two silicon atoms being 2.73 Å. T and H configurations are both stable, albeit with large insertion energies of 10.22 eV and 10.82 eV. Finally, the split interstitial SP is not stable, the BC configuration being obtained after relaxation.

Like for krypton, the xenon atom prefers to stay at the center of the monovacancy, with $E_i = 3.34$ eV. The final structure keeps the T_d symmetry, and is characterized by a maximum displacement of 0.79 Å for the silicon atoms first-neighbors of the vacancy. Like for argon and krypton, these atoms appear to be in a sp^2 hybridized state. Considering finally the divacancy, we found that both V_2C and V_2S configurations were stable, with very close insertion energies of 2.54 eV and 2.30 eV, respectively (Table 1). Both configurations have then a similar occurence probability.

Like for all NG species, save helium, vacancies will trap the xenon atom. The Fig. 6 also shows that the thermally activated formation of vacancies in close vicinity to the xenon location is now clearly energetically favored. The thermal formation of divacancies also becomes competitive. This suggests that a xenon atom in interstitial configuration will have a short lifetime.

4. Model

In the Table 1, there is an obvious relation between the weight of the NG impurity and the magnitude of the associated insertion energies. The heavier NG species are also those for which spatial delocalization of electrons is the largest. Then it is convenient to say that the bulkiest NG atoms require the largest energies to be introduced into silicon. Taking into account that interactions between the NG impurity and silicon atoms are certainly purely repulsive, most favorable insertion sites should be the ones with the largest available free volumes. This concept has already been proposed in previous works [72,74,66]. However, this simple argument is not enough to explain available results. For instance, it has been shown that in iron and nickel the octahedral interstitial site, which offers the larger free space, is less favored than the tetrahedral interstitial site for helium [66]. The authors of this work proposed that introducing the helium atom in the tetrahedral site is energetically less expensive due to an easiest local deformation of the host lattice. One could think that this argument is even more valid for the heaviest NG species.

Another issue with the simple free volume argument is the high insertion energy in the case of helium. In fact, there is a non negligible energy difference of 0.82 eV in favor of the interstitial site compared to the monovacancy. It can hardly be explained on the basis of available volume, since their first-neighbors environments are the same. Then following Hepburn and co-workers [66], a possible explanation is the easiest local deformation of silicon around the tetrahedral site compared to the V_1S configuration. The analysis of relaxed structures reveals instead larger lattice deformations in the case of the interstitial site than for the substitutional one. However, introducing the helium atom into the monovacancy prevents its relaxation by the well known Jahn–Teller mechanism. It may explain the highest insertion energy for substitution, and be considered as a local distortion associated to the helium presence compared to the relaxed monovacancy. Another possible contribution is related to the repulsive interaction between the local electronic density and the NG impurity [98,70], an argument based on the effective medium theory [99], It has been shown that a nearly linear energy increase is obtained when a NG atom is embedded into an homogeneous electron gas of increasing density [98,100]. Our calculations indicate that the electronic density is equal to 0.00458 $bohr^{-3}$ in the tetrahedral site, and to 0.01173 $bohr^{-3}$ in the center of the monovacancy (Table 2). This difference is in agreement with a larger insertion energy for the substitutional helium atom.

The different points discussed above would suggest that the insertion energy E_i of a NG impurity could be expressed as the sum of two contributions, an elastic one and an electronic one:

$$E_i = E_{elec} + E_{elas} \tag{4}$$

In agreement with Ref. [98], we use a linear relation for E_{elec}:

$$E_{elec} = \alpha \times n \tag{5}$$

with n the local electronic density at the insertion site, and α a constant characteristic of each NG species [98]. The elastic contribution can be estimated using the following expression

$$E_{elas} = \frac{24\pi\mu\delta a^2 a}{3 + 4\mu\chi'} \tag{6}$$

which gives the elastic energy related to the insertion of a spherical inclusion of radius $r = a + \delta a$ and compressibility χ' into a spherical hole of radius a in a homogeneous medium of shear modulus μ [101]. To use this expression, we implicitly assume that a single NG atom could be equivalent to a homogeneous inclusion, and that isotropic elasticity theory is suitable here. These points will be discussed in details in the following. We also define that $E_{elas} = 0$ if $\delta a < 0$, i.e. if the size of the inclusion is smaller than the available free volume, since attractive interactions between the NG impurity and the matrix are negligible here.

Our general purpose is to determine whether this simple inclusion model could be suitable for reproducing the results of DFT calculations. There are three unknown quantities for each NG species, α, χ', and its radius $r = \delta a + a$. In addition, the radii a of the spherical holes associated to the available free volume at each insertion site, are also unknown. All these quantities have been fitted against the DFT computed insertion energies, using a simple Nelder-Mead algorithm. Insertion energies of stable T, H, V_1S, V_2S, and V_2C configurations were selected as targets during the optimization procedure. BC configurations have not been considered because the relaxed geometry is characterized by an important unidirectional distortion clearly incompatible with the spherical deformation assumption of the model. The electronic densities at the corresponding sites, extracted from the DFT calculations of pristine bulk, and of the silicon mono- and di-vacancy, are given in the Table 2. Finally, the shear modulus of silicon is taken equal to the Voigt average of 68 GPa [102]. The quantities resulting from the fit are reported in the Tables 2 and 3, while the Fig. 7 shows the correlation between insertion energies obtained with DFT and with the model. The latter clearly shows an excellent agreement between the reference DFT energies and the values obtained from Eq. 4. In

Table 2
DFT computed electronic density n (in $bohr^{-3}$) and fitted radius hole a (in Å) at each insertion site, in pristine silicon or for relaxed V_1 and V_2 configurations.

	T	H	V_1S	V_2C	V_2S
n	0.00458	0.00629	0.01173	0.00048	0.00964
a	1.08	0.87	2.03	2.01	2.20

Table 3
NG-related quantities $\alpha, 1/\chi'$, and r, as defined in the inclusion model, obtained by fitting DFT calculated insertion energies. r_{DFT} values have been determined from DFT-PBE calculations of fcc NG solids (see text for details).

	He	Ne	Ar	Kr	Xe
α (eV bohr^3)	160	171	161	46	101
$1/\chi'$ (GPa)	40	37	35	36	56
r (Å)	1.35	1.79	2.36	2.56	2.56
r_{DFT} (Å)	1.47	1.61	2.07	2.26	2.49

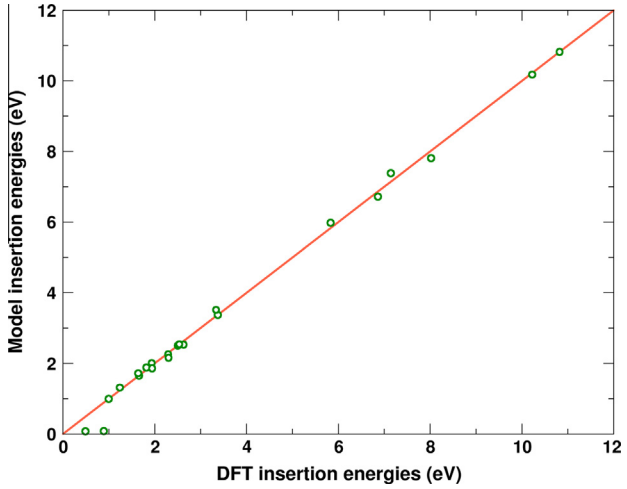

Fig. 7. Correlation plot between insertion energies calculated with the inclusion model and with DFT. The red straight line indicates equality ($y = x$). (For interpretation of the references to colour in this figure legend, the reader is referred to the web version of this article.)

most of cases, the differences are below 0.1 eV, the most divergent cases corresponding to helium and neon at the center of the divacancy (0.4 eV and 0.8 eV respectively).

The Fig. 8 shows the relative contributions of elastic and electronic terms to the insertion energy for the different investigated cases. There is a clear increase of the elastic part when going from the small helium to the large xenon, as expected. Also this figure reveals that the elastic contribution is the largest one for interstitial T and H configurations. Conversely, the main contribution in the case of the monovacancy is the electronic part. For helium and neon, this is even the only contribution to the insertion energy according to the model, which is in agreement with the negligible structural relaxation observed in those cases, and the fact that the center of the monovacancy is not the most stable site.

The success of the fitting procedure is an important prerequisite towards the validation of the model, but it is even more important to analyze the different resulting quantities. In fact, values out of meaningful range or even unphysical (e.g. negative compressibility) would be a clear indication that the above model is not appropriate. We begin our analysis with the computed α values (Table 2). For helium, our computed value is lower than previously published data [98,99] (275 eV bohr^3 and 313 eV bohr^3), but the order of magnitude is correct. For neon and argon, the computed values increase to 171 eV bohr^3 and 161 eV bohr^3 respectively. Still they are much lower than values reported in the Ref. [98]. One possible explanation lies in the use of LDA in these earlier calculations, which may lead to an overestimation of α due to a well known overbinding behavior. Furthermore, it is noteworthy that the linearity is lost in the low density range (< 0.002 eV bohr^3) for all NG species save helium [100], with much smoother slopes. In our case, this concerns the divacancy configurations (Table 2), and it is probably the reason why our computed α values are lower. It may also explain why the result of the fit is less satisfactory in the case of divacancy configurations. For krypton and xenon, α is now lower, although one could have expected the opposite [100]. Overall, we obtain reasonable α values with the expected order of magnitude for the light NG species. Although our values may appear too small for heavier NG species, this has a limited effect on the final result since the main contribution of the insertion energy is E_{elas} due to the large lattice distortions.

The second set of data concerns the compressibility of the inclusion χ', or more conveniently $1/\chi'$ the bulk modulus (Table 3). Obviously this is an ill-defined quantity in our case since the inclusion is a single atom. Nevertheless, it is possible to define an appropriate range of values. Considering first that the bulk modulus is related to the strength of the interatomic bonds, $1/\chi'$ is largely dependent on the strength of the interaction between the NG impurity and its silicon neighbors. NG species are notoriously known to be highly compressible (low bulk modulus) in fluid states, but data are scarce for solids. We have obtained a crude estimation of the bulk modulus of fcc solid NG species by performing DFT-PBE calculations (with the same cutoff than before and high density k-points grid). Resulting values are approximately 1–2 GPa, in good agreement with available data [103–106], and thus much lower than the bulk modulus of silicon equal to 100 GPa [102] as expected. It is then reasonable to assume that $1/\chi'$ values

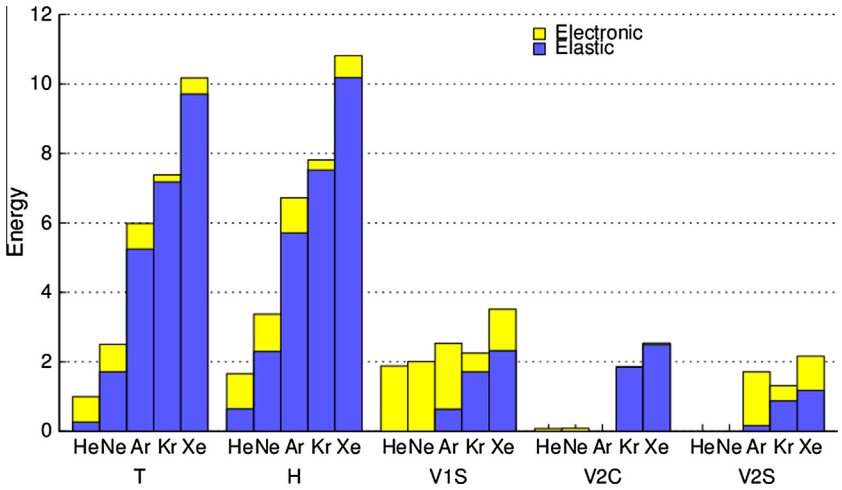

Fig. 8. Histogram plot showing the energy division between electronic (yellow) and elastic (blue) contributions in the model for the different configurations and NG species. (For interpretation of the references to colour in this figure legend, the reader is referred to the web version of this article.)

would range from 1 to 100 GPa. This is what we obtained during the fitting procedure, with values typically ranging from 35 GPa to 56 GPa. Therefore, calculated compressibility data further validate our model. It also suggests that taking the average of inverse compressibility may be a suitable approximation.

The last NG-related quantity is the radius r of the NG atom. This is also an ill-defined property, which necessarily depends on how the atom size is defined. For instance, it is possible to find atomic, covalent, van der Waals, ionic, and metallic radii values for many elements of the periodic table. In the case of NG, the van der Waals radius seems to be the most plausible option [107]. Nevertheless, there is a large scatter in available data, because van der Waals radii tend to vary with the particular chemical environment of the atom [108]. An alternative and consistent option is to consider the radius r_{DFT}, equal to half the first neighbors distance in the fcc NG crystal that we previously described. These values are reported in the Table 3, together with radii stemming from the fitting procedure. A good agreement is reached for helium, neon, and xenon. The largest differences of about 0.3 Å correspond to argon and krypton, which remains quite satisfactory. Again, this set of data validates our model.

Finally, the last quantities obtained from the fit are the radii of the spherical hole in the host lattice, which is dependent on the insertion site. The values resulting from the fit are reported in the Table 2. A reasonable number is obtained for the T site, since the fitted radius of 1.08 Å is slightly lower than half the distance to the first-neighbors silicon atoms (1.18 Å). In comparison, we also found a plausible value of 0.87 Å for the H site, in agreement with a smaller available space. However, surprisingly large values of 2.03 Å and 2.20 Å are obtained for the monovacancy center (V_1S) and a vacancy center in the divacancy (V_2S). An estimation of the available volume at these sites based on a first neighbors distance analysis would yield much lower equivalent radius, around 1.2 Å. This suggests that deforming the silicon lattice to insert a NG atom in V_1S and V_2S sites is easier than expected. This could be reproduced in the model only with large effective volumes to avoid too high elastic energies. At last, the fitted radius for the center of the divacancy site (V_2C) is found to be 2.01 Å, which corresponds to a reasonable equivalent volume for a divacancy.

In conclusion, the inclusion model proposed here seems to capture most of the physics related to the insertion of a NG atom into silicon, since reasonable values are obtained for almost all fitted quantities. One could be surprised of such a success, especially given the assumption of isotropic elasticity, and even more the modeling of an embedded single atom by a spherical inclusion in a homogeneous medium. Only the insertion energies for helium and neon in the center of the divacancy are too low compared to DFT computed results (Fig. 7). But this is not a dramatic issue since it does not change the stability ordering of the possible configurations. However it is noteworthy that we did not use the most stable BC configuration for argon, krypton and xenon in the fitting procedure. Considering that the available space for inserting a NG atom between two first neighbors silicon atoms is necessarily very small, and that the electronic density should be high at this site, very high insertion energies would be obtained with the inclusion model, in stark contrast with DFT calculated data. This is clearly a failure, the initial model assumptions being not compatible with large unidirectional deformations concentrated on only two atoms. Then, it appears that this inclusion model would be best suited for light small NG species such as helium and neon.

Besides, it would be interesting to check the performance of this model for other materials. Obviously, considering other cubic diamond materials, for which the equivalent radii at each possible sites have been determined here (Table 2), is straightforward. As a test, the inclusion model was then used to determine the insertion energy in T and H sites for helium and neon in diamond, for which values are available [79]. Equivalent radii for T and H sites were scaled accordingly to the ratio between diamond and silicon lattice constants. We assumed that charge densities are roughly the same at T and H sites for both materials. Finally, for elasticity constants, we considered the experimental shear modulus of 478 GPa, and the inverse compressibility of the inclusion was chosen to be 221 GPa. The latter is estimated as the arithmetic average of bulk moduli of diamond (442 GPa) and of the DFT-computed NG solid (1–2 GPa), as previously discussed. For helium, Goss and co-workers [79] found insertion energies of 6.3 eV (T) and 8.6 eV (H), while our model predicts 6.37 eV (T) and 7.72 eV (H). The agreement is excellent for the T site, and only 10% too low for the H site. For neon, values of 16.84 eV (T) and 17.52 eV are determined with the model, slightly lower than the published data (17.9 eV (T) and 19.5 eV (H)). Overall, the differences are less than 10%, which is really encouraging given the approximate choice of diamond parameters. In a larger perspective, this model may be even more appropriate to predict the behavior of NG in metallic materials. In fact, the assumption of a spherical inclusion in an isotropic medium is probably more difficult to use in materials with covalent bonds, which may favor higly distorted anisotropic deformations. Nonetheless, this point would require further investigations.

5. Conclusion

This paper reports on our investigations concerning the stability properties of single NG atoms in pristine silicon, and in interaction with a mono- and a divacancy. Structures and energies associated with several possible configurations have been obtained by performing DFT-PBE calculations.

Our calculations first confirmed that the most stable configuration for helium and neon interstitials was the tetrahedral T site. Besides, we found a new stable configuration for argon, krypton, and xenon, similar to the bond-centered structure favored for atomic hydrogen. For argon, it is as stable than the T configuration, whereas it becomes much more stable than all alternatives for krypton and xenon. We showed that mono- and divacancies were traps for all NG species, save helium which is repelled by the monovacancy. Another singularity is found for neon which is best located in the vicinity of the monovacancy, unlike heavier NG species. In conditions of vacancy supersaturation, interstitial NG atoms are then expected to be captured. Comparing the interstitial insertion with a process involving the thermally activated formation of vacancies, it appears that the latter becomes more and more likely for larger NG species. Hence, for krypton and xenon, the lifetime of interstitial configurations is predicted to be very short, even in a non-damaged material.

In a second part, we proposed a model combining a repulsive interaction between the host local electronic density and the NG impurity, and an elastic description of the NG atom as a deformable spherical inclusion into an homogeneous isotropic medium. The different parameters of this model, either being an intrinsic property of the NG atom or pertaining to the silicon host, have been fitted against several DFT-computed insertion energies, and the analysis of the final numbers suggests that the model is appropriate to describe the embedding of a helium or neon atom into silicon. Using approximated data, we showed that the model can be used to determine energies for interstitial helium and neon in diamond with a good accuracy.

Acknowledgements

M.-L. David, E. Oliviero, M.-F. Beaufort, J.-F. Barbot, and M. Bertolus are gratefully acknowledged for fruitful discussions. Figs. 1–5 were made with VMD software support. VMD is developed with

NIH support by the Theoretical and Computational Biophysics group at the Beckman Institute, University of Illinois at Urbana-Champaign.

References

[1] S.E. Donnelly, J.H. Evans (Eds.), Fundamental Aspects of Inert Gases in Solids, Plenum, 1991.
[2] V. Raineri, A. Battaglia, E. Rimini, Nucl. Instrum. Methods Phys. Res. B 96 (1995) 249.
[3] V. Raineri, M. Saggio, E. Rimini, J. Mater. Res. 15 (7) (2000) 1449.
[4] P.R. Heck, K.K. Marhas, P. Hoppe, R. Gallino, H. Baur, R. Wieler, Astrophys. J. 656 (2007) 1208.
[5] G.F. Cerofolini, F. Corni, S. Frabboni, C. Nobili, G. Ottaviani, R. Tonini, Mater. Sci. Eng. Rep. 27 (2000) 1.
[6] S.E. Donnelly, Radiation Effects 90 (1985) 1.
[7] H. Trinkaus, B. Singh, J. Nucl. Mater. 323 (2003) 229.
[8] C. Griffioen, J. Evans, P.D. Jong, A. van Veen, Nucl. Instrum. Methods Phys. Res. B 27 (1987) 417.
[9] F. Corni, C. Nobili, G. Ottaviani, R. Tonini, G. Calzolari, G. Cerofolini, G. Queirolo, Phys. Rev. B 56 (12) (1997) 7331.
[10] P.F.P. Fichtner, J.R. Kaschny, M. Behar, R.A. Yankov, A. Mücklich, W. Skorupa, Nucl. Instrum. Methods Phys. Res. B 148 (1999) 329.
[11] G. Cerofolini, G. Calzolari, F. Corni, S. Frabboni, C. Nobili, G. Ottaviani, R. Tonini, Phys. Rev. B 61 (15) (2000) 10183.
[12] E. Oliviero, M.-L. David, M.-F. Beaufort, J.-F. Barbot, A. van Veen, Appl. Phys. Lett. 81 (22) (2002) 4201.
[13] M.-L. David, M.-F. Beaufort, J.-F. Barbot, J. Appl. Phys. 93 (3) (2003) 1438.
[14] S. Frabboni, F. Corni, C. Nobili, R. Tonini, G. Ottaviani, Phys. Rev. B 69 (2004) 165209.
[15] K. Hojou, K. Izui, J. Nucl. Mater. 160 (1988) 147.
[16] J. Chen, P. Jung, H. Trinkaus, Phys. Rev. B 61 (19) (2000) 12923.
[17] P. Jung, H. Klein, J. Chen, J. Nucl. Mater. 283–287 (2000) 806.
[18] E. Oliviero, M.-F. Beaufort, F. Pailloux, J.-F. Barbot, Nucl. Instrum. Methods Phys. Res. B 218 (2004) 391.
[19] L. Vincent, T. Sauvage, G. Carlot, P. Garcia, G. Martin, M.-F. Barthe, P. Desgardin, Vacuum 83 (2009) S36.
[20] J.-F. Barbot, F. Pailloux, M.-L. David, L. Pizzagalli, E. Oliviero, G. Lucas, J. Appl. Phys. 104 (2008) 043526.
[21] M.-F. Beaufort, L. Pizzagalli, A.S. Gandy, E. Oliviero, D. Eyidi, et S.E. Donnelly, J. Appl. Phys. 104 (2008) 094905.
[22] M.-F. Beaufort, J.-F. Barbot, M. Drouet, S. Peripolli, E. Oliviero, L. Amaral, P. Fichtner, Nucl. Instrum. Methods Phys. Res. B 257 (2007) 750.
[23] C. Zhang, Y. Sun, Y. Song, T. Shibayama, Y. Jin, L. Zhou, Nucl. Instrum. Methods Phys. Res. B 256 (2007) 243.
[24] W. Sawyer, J. Weber, G. Nabert, J. Schmalzlin, H. Habermeier, J. Appl. Phys. 68 (1990) 6179.
[25] G. Faraci, S.L. Rosa, A.R. Pennisi, S. Mobilio, G. Tourillon, Phys. Rev. B 43 (12) (1991) 9962.
[26] R. Dhaka, C. Biswas, A. Shukla, S. Barman, A. Chakrabarti, Phys. Rev. B 77 (2008) 104119.
[27] B. Li, C. Zhang, Y. Zhong, D. Wang, L. Zhou, Y. Yang, H. Zhang, L. Zhang, Nucl. Instrum. Methods Phys. Res. B 267 (14) (2009) 2395–2398. http://dx.doi.org/10.1016/j.nimb.2009.05.004. <http://www.sciencedirect.com/science/article/pii/S0168583X09005564>.
[28] B. Li, C. Zhang, Y. Yang, L. Zhang, C. Xu, Appl. Surf. Sci. 257 (21) (2011) 9183–9187. http://dx.doi.org/10.1016/j.apsusc.2011.05.129. <http://www.sciencedirect.com/science/article/pii/S0169433211008592>.
[29] L. Pagano Jr., A. Motta, R. Birtcher, J. Nucl. Mater. 244 (1997) 295.
[30] G. Faraci, A. Pennisi, J.-L. Hazemann, Phys. Rev. B 56 (19) (1997) 12553.
[31] C. Templier, B. Boubeker, H. Garem, E.L. Math, J.C. Desoyer, Phys. Stat. Sol. a 92 (1985) 511.
[32] G. Faraci, A. Pennisi, F. Zontone, B. Li, I. Petrov, Phys. Rev. B 74 (2006) 235436.
[33] H. Assaf, E. Ntsoenzok, M.-F. Barthe, M.-O. Ruault, T. Sauvage, S. Ashok, Nucl. Instrum. Methods Phys. Res. B 253 (2006) 222.
[34] H. Trinkaus, Radiation Effects 78 (1983) 189.
[35] A.V. Felde, J. Fink, T. Müller-Heinzerling, J. Pflüger, B. Scheerer, G. Linker, D. Kaletta, Phys. Rev. Lett. 53 (9) (1984) 922.
[36] N. Hueging, M. Luysberg, H. Trinkaus, K. Tillmann, K. Urban, J. Mater. Sci. 41 (2006) 4454.
[37] D. Taverna, M. Kociak, O. Stéphan, A. Fabre, E. Finot, B. Décamps, C. Colliex, Phys. Rev. Lett. 100 (2008) 035301.
[38] S. Fréchard, M. Walls, M. Kociak, J. Chevalier, J. Henry, D. Gorse, J. Nucl. Mater. 393 (2009) 102.
[39] M. Maekawa, A. Kawasuso, J. Phys. Conf. Ser. 225 (2010) 012032.
[40] M.-L. David, F. Pailloux, V. Mauchamp, L. Pizzagalli, Appl. Phys. Lett. 98 (2011) 171903.
[41] K. Morishita, R. Sugano, B.D. Wirth, T. Diaz de la Rubia, Nucl. Instrum. Methods Phys. Res. B 202 (2003) 76.
[42] S.M. Valones, M.I. Baskes, R.L. Martin, Phys. Rev. B 73 (2006) 214209.
[43] H.-Y. Wang, W.-J. Zhu, S.-J. Liu, Z.-F. Song, X.-L. Deng, X.-R. Chen, H.-L. He, Nucl. Instrum. Methods Phys. Res. B 267 (2009) 849.
[44] S.H. Haghighat, G. Lucas, R. Schäublin, Europhys. Lett. 85 (2009) 60008.
[45] G. Lucas, R. Schäublin, J. Nucl. Mater. 386–388 (2009) 360.
[46] A. Couet, J.-P. Crocombette, A. Chartier, J. Nucl. Mater. 404 (2010) 50.
[47] Z. Bao-Ling, W. Jun, H. Qing, Chin. Phys. B 20 (3) (2011) 036105.
[48] A. Caro, J. Hetherly, A. Stukowski, M. Caro, E. Martinez, S. Srivilliputhur, L. Zepeda-Ruiz, M. Nastasi, J. Nucl. Mater. 418 (1–3) (2011) 261–268, http://dx.doi.org/10.1016/j.jnucmat.2011.07.010. <http://www.sciencedirect.com/science/article/pii/S0022311511006623>.
[49] L. Pizzagalli, M.L. David, M. Bertolus, Modell. Simul. Mater. Sci. Eng. 21 (6) (2013) 065002. <http://stacks.iop.org/0965-0393/21/i=6/a=065002>.
[50] B. Zhang, J. Wang, M. Li, Q. Hou, J. Nucl. Mater. 438 (13) (2013) 178–182. http://dx.doi.org/10.1016/j.jnucmat.2013.03.033. <http://www.sciencedirect.com/science/article/pii/S0022311513005357>.
[51] W. Windl, T.J. Lenosky, J.D. Kress, A.F. Voter, Nucl. Instrum. Methods Phys. Res. B 141 (1998) 61.
[52] G. Lucas, L. Pizzagalli, Phys. Rev. B 72 (2005) 161202R.
[53] G. Lucas, L. Pizzagalli, Nucl. Instrum. Methods Phys. Res. B 229 (2005) 359.
[54] E. Holmström, A. Kuronen, K. Nordlund, Phys. Rev. B 78 (2008) 045202.
[55] G. Lucas, L. Pizzagalli, J. Phys.: Condens. Matter 19 (2007) 086208.
[56] G. Lucas, L. Pizzagalli, Nucl. Instrum. Methods Phys. Res. B 25 (2007) 124.
[57] W.D. Wilson, C.L. Bisson, M.I. Baskes, Phys. Rev. B 24 (24) (1981) 5616.
[58] C.-C. Fu, F. Willaime, Phys. Rev. B 72 (2005) 064117.
[59] C. Becquart, C. Domain, Phys. Rev. Lett. 97 (2006) 196402.
[60] T. Seletskaia, Y. Osetsky, R. Stoller, G. Stocks, J. Nucl. Mater. 351 (2006) 109.
[61] X.T. Zu, L. Yang, F. Gao, S.M. Peng, H.L. Heinisch, X.G. Long, R.J. Kurtz, Phys. Rev. B 80 (2009) 054104, http://dx.doi.org/10.1103/PhysRevB.80.054104. <http://link.aps.org/doi/10.1103/PhysRevB.80.054104>.
[62] C.S. Becquart, C. Domain, J. Nucl. Mater. 386–388 (2009) 109.
[63] Y.-l. Wang, S. Liu, L.-j. Rong, Y.-m. Wang, J. Nucl. Mater. 402 (1) (2010) 55–59. http://dx.doi.org/10.1016/j.jnucmat.2010.04.022. <http://www.sciencedirect.com/science/article/pii/S0022311510001662>.
[64] L. Yang, S. Peng, X. Long, F. Gao, H. Heinisch, R. Kurtz, X. Zu, J. Phys.: Condens. Matter 23 (2011) 035701.
[65] A.S. Bakai, A.N. Timoshevskii, B.Z. Yanchitsky, Low Temp. Phys. 37 (9–10) (2011) 791.
[66] D.J. Hepburn, D. Ferguson, S. Gardner, G.J. Ackland, Phys. Rev. B 88 (2013) 024115, http://dx.doi.org/10.1103/PhysRevB.88.024115. <http://link.aps.org/doi/10.1103/PhysRevB.88.024115>.
[67] R. Li, P. Zhang, C. Zhang, X. Huang, J. un Zhao, J. Nucl. Mater. 440 (13) (2013) 557–561. http://dx.doi.org/10.1016/j.jnucmat.2013.03.068. <http://www.sciencedirect.com/science/article/pii/S0022311513005710>.
[68] Y. Yun, O. Eriksson, P. Oppeneer, H. Kim, K. Park, J. Nucl. Mater. 385 (2009) 364.
[69] J. Xiao, C. Wang, T. Yang, S. Kong, J. Xue, Y. Wang, Nucl. Instrum. Methods Phys. Res. B 304 (0) (2013) 27–31. http://dx.doi.org/10.1016/j.nimb.2013.04.006. <http://www.sciencedirect.com/science/article/pii/S0168583X13004035>.
[70] M. Alatalo, M.J. Puska, R.M. Nieminen, Phys. Rev. B 46 (19) (1992) 12806.
[71] W.R. Allen, J. Nucl. Mater. 210 (1994) 318.
[72] S.K. Estreicher, J. Weber, A. Derecskei-Kovacs, D.S. Marynick, Phys. Rev. B 55 (8) (1997) 5037.
[73] V.G. Zavodinsky, A.A. Gnidenko, A. Misiuk, J. Bak-Misiuk, Vacuum 78 (2005) 247.
[74] A. Charaf Eddin, G. Lucas, M.F. Beaufort, L. Pizzagalli, Comput. Mater. Sci. 44 (2009) 1030.
[75] R.M.V. Ginhoven, A. Chartier, C. Meis, W.J. Weber, L.R. Corrales, J. Nucl. Mater. 348 (2006) 51.
[76] J.H. Kim, Y.D. Kwon, P. Yonathan, I. Hidayat, J.G. Lee, J.-H. Choi, S.-C. Lee, J. Mater. Sci. 44 (2009) 1828.
[77] W. Cheng, M.-J. Ying, F.-S. Zhang, H.-Y. Zhou, S.-F. Ren, Nucl. Instrum. Methods Phys. Res. B 269 (2011) 2067.
[78] A. Charaf Eddin, L. Pizzagalli, J. Nucl. Mater. 429 (13) (2012) 329–334. http://dx.doi.org/10.1016/j.jnucmat.2012.06.022. <http://www.sciencedirect.com/science/article/pii/S002231151200311X>.
[79] J. Goss, R. Eyre, P. Briddon, A. Mainwood, Phys. Rev. B 80 (2009) 085204.
[80] P. Giannozzi, S. Baroni, N. Bonini, M. Calandra, R. Car, C. Cavazzoni, D. Ceresoli, G.L. Chiarotti, M. Cococcioni, I. Dabo, A. Dal Corso, S. de Gironcoli, S. Fabris, G. Fratesi, R. Gebauer, U. Gerstmann, C. Gougoussis, A. Kokalj, M. Lazzeri, L. Martin-Samos, N. Marzari, F. Mauri, R. Mazzarello, S. Paolini, A. Pasquarello, L. Paulatto, C. Sbraccia, S. Scandolo, G. Sclauzero, A.P. Seitsonen, A. Smogunov, P. Umari, R.M. Wentzcovitch, J. Phys.: Condens. Matter 21 (39) (2009) 395502. <http://www.quantum-espresso.org>.
[81] Http://www.quantum-espresso.org/.
[82] P. Hohenberg, W. Kohn, Phys. Rev. 136 (3B) (1964) B864.
[83] W. Kohn, L.J. Sham, Phys. Rev. 140 (4A) (1965) A1133.
[84] J.P. Perdew, K. Burke, M. Ernzerhof, Phys. Rev. Lett. 77 (18) (1996) 3865.
[85] D.C. Patton, M.R. Pederson, Phys. Rev. A 56 (1997) R2495.
[86] D. Vanderbilt, Phys. Rev. B 41 (11) (1990) 7892.
[87] H.J. Monkhorst, J.D. Pack, Phys. Rev. B 13 (12) (1976) 5188.
[88] S. Dannefaer, P. Mascher, D. Kerr, Phys. Rev. Lett. 56 (20) (1986) 2195.
[89] M.J. Puska, S. Pöykkö, M. Pesola, R.M. Nieminen, Phys. Rev. B 58 (3) (1998) 1318.
[90] F. El-Mellouhi, N. Mousseau, P. Ordejón, Phys. Rev. B 70 (2004) 205202.
[91] G.D. Watkins, J.W. Corbet, Phys. Rev. 138 (2A) (1965) A543.
[92] J.L. Hastings, S.K. Estreicher, P.A. Fedders, Phys. Rev. B 56 (16) (1997) 10215.
[93] D. Caliste, P. Pochet, Phys. Rev. Lett. 97 (2006) 135901.
[94] C.G. van de Walle, P.J.H. Denteneer, Y. Bar-Yam, S.T. Pantelides, Phys. Rev. B 39 (15) (1989) 10791.

[95] S.K. Estreicher, M.A. Roberson, D.M. Maric, Phys. Rev. B 50 (23) (1994) 17018.
[96] V. Raineri, S. Coffa, E. Szilágyi, J. Gyulai, E. Rimini, Phys. Rev. B 61 (2) (2000) 937.
[97] A. Charaf Eddin, L. Pizzagalli, J. Phys.: Condens. Matter 24 (2012) 175006.
[98] M.J. Puska, R.M. Nieminen, M. Manninen, Phys. Rev. B 24 (6) (1981) 3037.
[99] M.J. Stott, E. Zaremba, Phys. Rev. B 22 (1980) 1564–1583, http://dx.doi.org/10.1103/PhysRevB.22.1564. http://link.aps.org/doi/10.1103/PhysRevB.22.1564.
[100] M.J. Puska, R.M. Nieminen, J. Phys.: Condens. Matter 3 (30) (1991) 5711–5721. http://dx.doi.org/10.1088/0953-8984/3/30/004.
[101] T. Mura, Micromechanics of Defects in Solids, second ed., Martinus Nijhoff Publishers, Dordrecht, The Netherlands, 1987.
[102] J.P. Hirth, J. Lothe, Theory of Dislocations, Wiley, New York, 1982.
[103] D.C. Wallace, Thermodynamics of Crystals, John Wiley and Sons, New York, 1970.
[104] M. Anderson, R. Fugate, C. Swenson, J. Low Temp. Phys. 10 (3/4) (1973) 345.
[105] M. Klein, J. Venables (Eds.), Rare Gas Solids, Academic Press, London, 1976.
[106] C. Herrero, J. Phys.: Condens. Matter 20 (2008) 295230.
[107] J.K. Badenhoop, F. Weinhold, J. Chem. Phys. 107 (14) (1997) 5422–5432. http://dx.doi.org/10.1063/1.475149. <http://scitation.aip.org/content/aip/journal/jcp/107/14/10.1063/1.475149>.
[108] A. Bondi, J. Phys. Chem. 68 (3) (1964) 441–451, http://dx.doi.org/10.1021/j100785a001.